Synthesis of α-MoO_3 nanofibers for enhanced field-emission properties

Sandeep Kumar Singh Patel,[1,*] Khemchand Dewangan,[2,*] Simant Kumar Srivastav,[3] Narendra Kumar Verma,[1] Paramananda Jena,[1] Ashish Kumar Singh,[1] N. S. Gajbhiye[3]

[1]*School of Materials Science and Technology, Indian Institute of Technology (Banaras Hindu University) Varanasi 221005, India*
[2]*Department of Chemistry, Indira Gandhi National Tribal University, Amarkantak 484886, India*
[3]*Department of Chemistry, Indian Institute of Technology, Kanpur 208016, India*

*Corresponding author

DOI: 10.5185/amlett.2018.2022
www.vbripress.com/aml

Abstract

One-dimensional α-MoO_3 nanofibers of 280–320 nm diameters were synthesized by a hydrothermal method. The morphologies and compositions of as-synthesized α-MoO_3 nanofibers have been characterized by X-ray powder diffraction, Raman spectroscopy, and field-emission scanning electron microscopy. X-ray photoelectron spectroscopy showed the predominantly 6+ oxidation state with a small percentage of reduced δ+ ($5 < \delta < 6$) oxidation state. The field-emission properties of α-MoO_3 nanofibers show a lower turn-on electric field of 2.48 V μm^{-1} and threshold electric field of 3.10 V μm^{-1}. The results suggest that the α-MoO_3 nanofibers are promising candidate for efficient and high-performance field-emission devices. Copyright © 2018 VBRI Press.

Keywords: Nanofibers; molybdenum oxide; hydrothermal method; field emission properties.

Introduction

One-dimensional (1D) nanostructures have been the subject of extensive research over few decades due to their peculiar and fascinating properties with novel applications **[1-3].** Moreover, the flexibility, shape anisotropy, extraordinary lengths and high surface to volume ratio of these nanostructures explore the use from electronic to photonic devices **[4-8].** Different sizes and morphology of the semiconductor nanostructures are reported for the potential application of field emitters such as field-effect transistors, lasers diodes, sensors, and photovoltaic cells **[9-11].**

Recently, the α-MoO_3 one of the utmost stable form of the molybdenum metal oxide semiconductor (band-gap = 3.8 eV), shows a remarkable attention due to extensive potential applications in photoconductive, thermoelectric, pseudocapacitors, Li-ion intercalation-deintercalation and field-emission devices [**12,13].** Now a days field-emission, is one of the commercial attention for electronic and display devices. Further 1D nanostructure is one of the prominent features for the field-emission in the viewpoint of application. It has enhanced the interest in the synthesis methods as well as electrochemical properties of 1D semiconductor nanostructures. In the past decades, field-emission properties are investigated from different 1D shapes of MoO_3 **[14-17]**. Yan *et al.* **[14]** have demonstrated that MoO_3 nanoflakes fabricated by modified hot plate method showed enhanced electron field-emission and reduced turn-on fields. Li *et al.* **[15]** have reported an improved field-emission property from the MoO_3 nanobelts synthesized by infrared irradiation heating a Mo foil in the air. Zhou *et al.* **[17]** have fabricated MoO_3 nanowires via thermal evaporation method followed by further oxidation, and this nanowire exhibited better field-emission than MoO_3 nanoflakes **[14]** and nanobelts arrays **[15]**. It is clear from the above report that the material with sharp tips and high aspect ratio can significantly increase field-emission performance **[14-17]**. Thus nanofibers are expected to possess a better field-emission property owing to their high aspect ratio, exposed sharp edges and low dimension geometry. It is still challenging task for the enhancement of field-emission properties in α-MoO_3 to meet viable applications required for flat displays, X-ray sources and development of microwave circuits.

In present study, we report a facile synthesis method for preparing α-MoO_3 nanofibers. The field-emission properties of the prepared nanofibers were investigated. These α-MoO_3 nanostructures shows excellent field-emission properties with stable emission behavior and low turn-on electric fields.

Experimental

The α-MoO_3 nanofibers were synthesized as per our previously reported method **[13]**. A freshly prepared 0.7 g polymeric nitrosyl-complex of molybdenum (II) **[18]** was dissolved in a mixture of 35 mL distilled water and

concentrated HNO_3 under constant stirring. The resulting yellowish-orange colored solution was transferred into an autoclave and then heated in a furnace at 220°C for 7 h. The obtained material was cooled to room temperature and thoroughly washed with deionized water and ethanol. The samples were collected and dried at 60 °C for 5 h.

The crystal structures were examined by X-ray diffraction (XRD) using a Rich Seifert Isodebyflex diffractometer with Cu-Kα (λ = 1.5418 Å) radiation. The vibrational modes of α-MoO_3 were characterized by Raman spectrometer (WITec Alpha_SNOM, λ = 532 nm line laser as excitation source). A field-emission scanning electron microscope (FESEM) FEI Quanta-200 was used to analyze the morphology of the sample. The chemical composition was analyzed using X-ray photoelectron spectroscopy (XPS) (SPECS, Phoibos 100 MCD Energy Analyzer). The field-emission studies were done by 'close proximity' (also termed as 'planar diode') set up using ultrahigh vacuum (~1×10^{-8} Torr pressure). As synthesized α-MoO_3 nanofibers deposited onto tungsten substrate (1×1 cm^2) by drop-casting method. Tungsten and copper were used as a cathode and an anode, respectively. The separation between cathode and anode was fixed at 250 µm by using alumina spacer. Keithley 485 Pico ammeter was used to carry out for the current density–applied field (*J–E*) measurements.

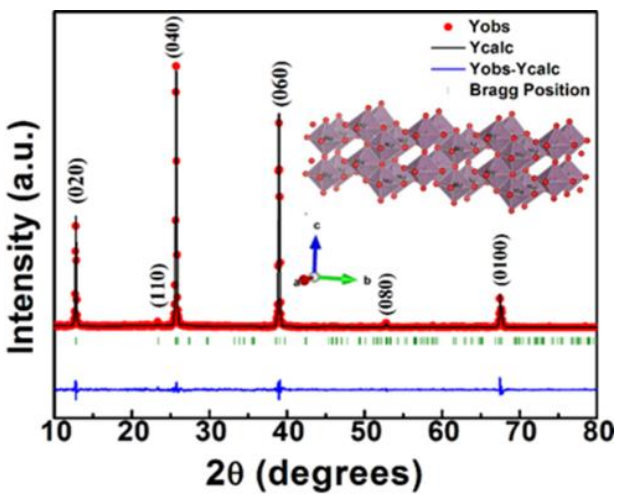

Fig. 1. Rietveld analysis of XRD data using orthorhombic structure with space group Pbnm of α-MoO_3 nanofibers and the insert shows the unit cell crystal structure.

Results and discussion

Fig. 1 depicts the Rietveld-refined XRD pattern of α-MoO_3 powder, which is indexed as the orthorhombic crystal system of MoO_3 having Pbnm space group (JCPDS card No. 76-1003). In XRD, a collimated X-ray beam with wavelength, λ are incident upon a crystalline sample and is diffracted according to the Bragg's law **[19]**:

$$2d \sin\theta = n\lambda$$

where *d* is the atomic spacing of two planes, θ is the diffraction angle and *n* is the order of diffraction. The lattice parameters for the orthorhombic crystal system ($a \neq b \neq c$ and $\alpha = \beta = \gamma = 90°$) are related to the *d*-spacing of the (*hkl*) planes as given by the equation:

$$\frac{1}{d^2} = \frac{h^2}{a^2} + \frac{k^2}{b^2} + \frac{l^2}{c^2}$$

where *h*, *k* and *l* are the Miller indices of the planes. The obtained lattice parameters are: a = 3.9623, b = 13.8576 and c = 3.6962 Å, respectively and the unit cell volume is 202.9508 $Å^3$. Reliability factors for the fit are R_p = 13.8%, R_{wp} = 25.6 %, R_{exp} = 18.32 % and χ^2 = 1.95. The XRD pattern shows that all other peaks except for (0k0) have very weak intensity in contrast to standard data. The observed intensities of reflection peaks of (020), (040), (060), (080) and (0100) are very strong, indicating the anisotropic morphology growth and preferential orientation of the α-MoO_3 nanofibers along the [001] direction **[13]**.

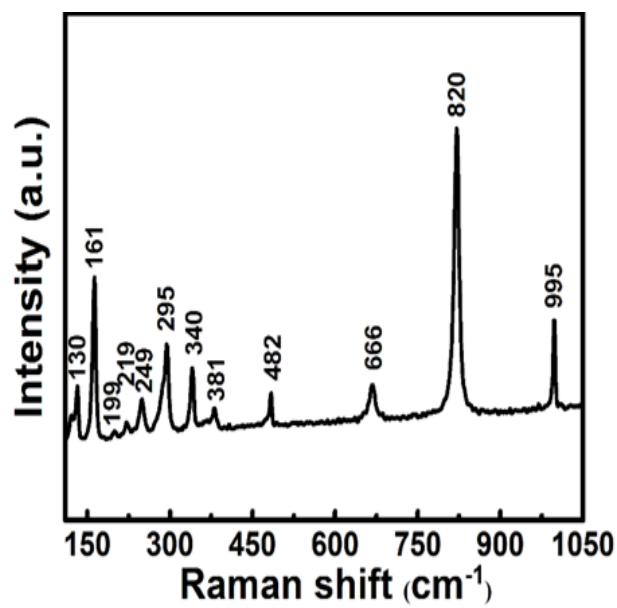

Fig. 2. Raman spectra of the α-MoO_3 nanofibers.

Micro-Raman spectra of α-MoO_3 nanofibers were collected under 532 nm excitation which is shown in **Fig. 2.** The observed band positions of obtained α-MoO_3 nanofibers are shown in **Table 1.** The Raman modes for α-MoO_3 can be written as;

$$\Gamma = 8A_g + 8B_{1g} + 4B_{2g} + 4B_{3g} + 4A_u + 3B_{1u} + 7B_{2u} + 7B_{3u}$$

where A_g, B_{1g}, B_{2g}, B_{3g} are Raman active, A_u is an inactive, and others are infrared-active modes **[20].** These modes are consistent with those in molybdenum trioxide reported by Lupan et al. **[20]** as shown in **Table 1.** Detailed Raman vibrational analysis of α-MoO_3 bands can be found elsewhere **[8,21,22]**.

Table 1. Peak position for the Raman modes (cm^{-1}) in our study on α-MoO_3 nanofibers in comparison to the reported data on α-MoO_3 nano-microribbons by Lupan *et al*. **[20]**

Raman modes	α-MoO_3 (our study)	Lupan et al.
B_{2g}	130	112
A_g, B_{1g}	161	154
B_{2g}	199	194
A_g	219	213
B_{3g}	249	-
B_{2g}, B_{3g}	295	280
B_{1g}, A_g	340	333
A_g	381	375
A_g, B_{1g}	482	469
B_{2g}, B_{3g}	666	662
A_g, B_{1g}	820	815
A_g, B_{1g}	995	991

Fig. 3 shows the low and high-resolution FESEM images of α-MoO_3 nanostructures. As shown in **Fig. 3**, α-MoO_3 nanostructures have fiber-like shape, which is distinct from those of nanowires and nanotubes, indicating that the hydrothermal method is an efficient method to synthesize the 1D nanostructures. The diameters of the α-MoO_3 nanofibers are between 280-320 nm and lengths greater than 5 µm.

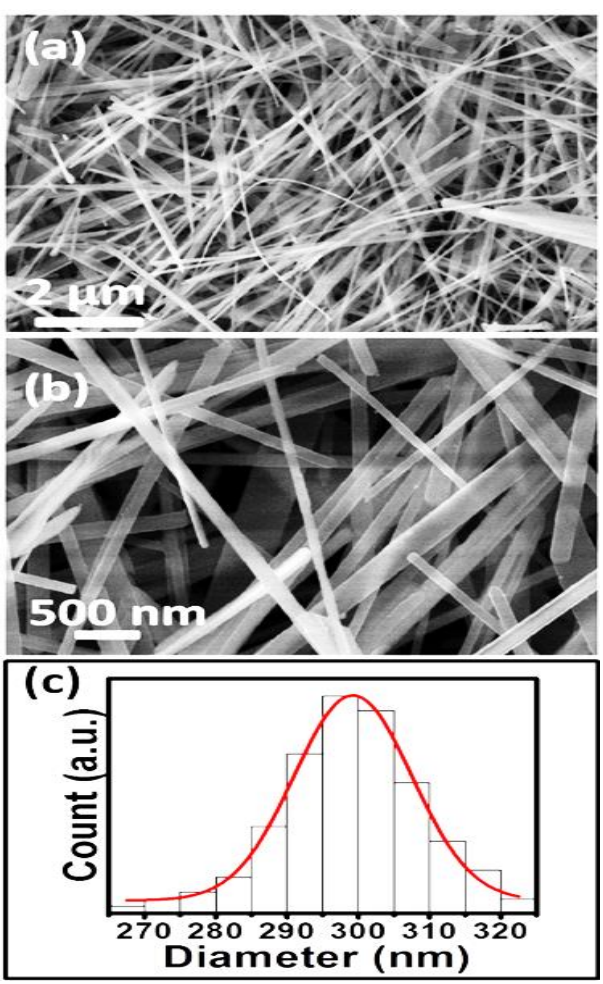

Fig. 3. FESEM images (a) low, (b) high-magnification and (c) histogram for the width distribution of the α-MoO_3 nanofibers.

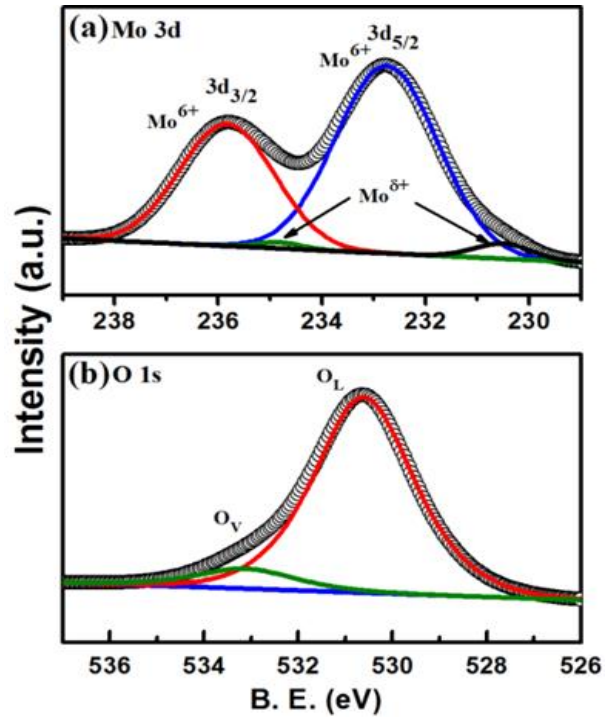

Fig. 4. XPS spectra of the (a) Mo 3d and (b) O 1s core level in α-MoO_3 nanofibers.

Fig. 4 shows the X-ray photoelectron spectroscopy (XPS) core level spectra of α-MoO_3 nanofibers, calibrated by the C (1s) line (285.0 eV) binding energy. In **Fig. 4(a)** two different valence states of Mo (3d) in the α-MoO_3 are observed. The major contributing peaks at 232.7 eV ($3d_{5/2}$) and 235.8 eV ($3d_{3/2}$) corresponded to Mo^{6+}, while the small ones at 230.5 eV ($3d_{5/2}$) and 234.8 eV ($3d_{3/2}$) are assigned to the 3d doublet of $Mo^{\delta+}$ ($5< \delta <6$) **[8,23]** . It indicates the existence of dangling bond defects in α-MoO_3 where charges could be trapped **[8,23]**. The mixed valence state of Mo (Mo^{6+} and $Mo^{\delta+}$) is often followed by the introduction of oxygen vacancies to keep charge neutrality **[8,23]**. Asymmetric and broad peaks observed in the O 1s spectrum, as shown in **Fig. 4(b),** at 530.6 eV and 533.1 eV correspond to the skeletal oxygen (O_L) and oxygen vacancies (O_V), respectively **[23]**. Thus, the XPS result confirms that the α-MoO_3 possess the oxygen vacancies.

Fig. 5(a) depicts typical current density versus applied electric field (*J–E*) plot for the α-MoO_3 nanofibers. A reproducibly emission current density of ~15 $nAcm^{-2}$ is observed with an applied electric field of 1.76 $V\mu m^{-1}$. It is observed that the current density increases exponentially with increase in electric field and found to be of 100 μAcm^{-2} at an applied field of 4 $V\mu m^{-1}$. Hence, we could defined the turn on and threshold fields as the required electric fields to generate a current density of 1 and 10 µA cm^{-2}, respectively. Lower the value of turn-on field leads to better field-emission properties of the material. In the present study, the value of turn-on and threshold fields are found to be 2.48 and 3.10 $V\mu m^{-1}$, respectively. It

can be seen from the **Table 2**; these observed values are noticeably lower than the values reported for the MoO_3 nanoflakes **[14]**, nanobelts **[15]**, nanoflowers **[16]**, and aligned nanowires **[17]**.

The dependence of current density over the electric field is expressed by using Fowler–Nordheim (F–N) law **[24]:**

$$J = A\left(\frac{\beta^2 E^2}{\phi}\right)\exp\left(\frac{-B\phi^{3/2}}{\beta E}\right) \text{ or}$$

$$\ln\left(\frac{J}{E^2}\right) = \ln\left(\frac{A\beta^2}{\phi}\right) - \frac{B\phi^{3/2}}{\beta E}$$

The plot of $\ln(J/E^2)$ versus $(1/E)$ is termed as F–N plot and derived from experimental data for α-MoO_3 nanofibers is depicted in **Fig. 5(b)**. The linear nature of F–N plot shows that field-emission from α-MoO_3 nanofibers follows the quantum mechanical tunneling process **[14–17, 25, 26].** The field enhancement factor β is calculated by using the following equation:

$$\beta = \frac{(-6.83\times10^3\phi^{3/2})}{m}$$

where ϕ is the work function of emitted material in eV, which is at least about 5.7 eV for α-MoO_3 and m is the slope of the F–N plot [**27,28].** Using the slope (m = –21.38) of fitted straight line of the F–N plot (**Fig. 5(b)**), β is calculated and found to be 4347, which is very high. The low turn-on field (2.48 Vμm^{-1}) and high field-emission factor (β = 4347) indicated that the α-MoO_3 nanofibers could be expected to a wide range of significant applications such as field-emitters and flat-panel display devices [**14-17].**

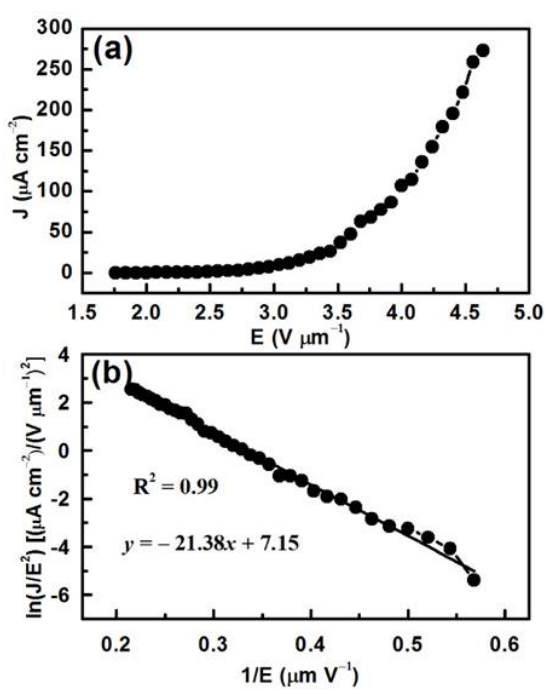

Fig. 5. Field-emission properties of α-MoO_3 nanofibers, (a) current versus electric fields (J–E), and (b) corresponding Fowler-Nordheim (F–N) plots with linear curve fitting (solid line).

Table 2. Field-emission performances of various α-MoO_3 nanostructures.

Emitter type	Turn-on field (V μm⁻¹)	Threshold field (V μm⁻¹)	β	Ref.
Nanoflakes	11.0	-	2500	14
Nanobelts	8.7	12.9	-	15
Nanoflowers	4.3	-	-	16
Nanowires	3.5	7.65	4400	17
Nanofibers	2.48	3.10	4347	[this work]

The reasons for our nanofibers possessed excellent field-emission properties may include the following. The low turn-on field and high value of β are attributed to the nanometric features of α-MoO_3 fibers apex and its high aspect ratio. Also, the defect oxygen vacancies may also play an essential role in describing the surface properties of α-MoO_3 nanofibers **[23]**. The presence of oxygen vacancies in α-MoO_3 nanofibers act as electron donors due to its n-type semiconducting nature. So these electron donors could shifts the Fermi energy level (E_f) up, which leads to lowered work function, as shown in **Fig. 6.** Thus the electron emission process increases due to decrease in the work function of the nanofibers **[29]**. Also the oxygen ions deficiency give rise to the reduction of the molybdenum ions, that increases the concentration of $Mo^{\delta+}$ (5< δ <6) ions, which decreases the work function **[29,30]**. Some further theoretical simulation can be expected to explain this field-emission behavior of α-MoO_3 nanofibers.

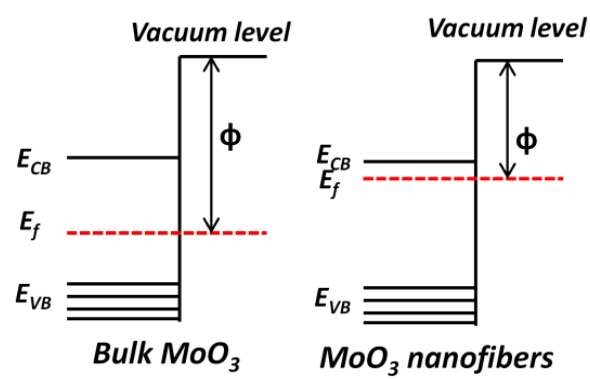

Fig. 6. Schematic diagram of energy levels for bulk MoO_3 and MoO_3 nanofibers. E_{CB}: conduction band. E_{VB}: valence band. E_f: Fermi level and ϕ: work function.

Conclusion

α-MoO_3 nanofibers having an orthorhombic crystal structure were synthesized by a hydrothermal method. The nanofibers are found to be of 280-300 nm in diameter and five to several μm in length. An extremely lower turn-on field (2.48 V μm^{-1}), smaller threshold field (3.10 V μm^{-1}) and high field-emission factor

(β = 4347) were obtained. Defect mediated (oxygen vacancies) field-emission was proposed to explain this phenomenon. This high-performance emission of α-MoO_3 nanofibers compared to other MoO_3 nanostructures is controllable, reproducible and can be applied for the development of practical electron sources in flat-panel display devices.

Acknowledgements

SKSP gratefully acknowledges to Science and Engineering Research Board (SERB) for providing National Post-Doctoral Fellowship (N-PDF). AKS thanks to DST for providing INSPIRE Faculty Fellowship.

References

1. Xia, Y.; Yang, P.; Sun, Y.; Wu, Y.; Mayers, B.; Gates, B.; Yin, Y.; Kim, F.;Yan, H.; *Adv. Mater.* **2003,** *15*, 353. **DOI:** 10.1002/adma.200390087
2. Kumar, P.R.; Khan, N.; Vivekanandhan, S.; Satyanarayana, N.; Mohanty, A. K.; Misra, M.; *J. Nanosci Nanotechnol.* **2012,** *12*, 1-25. **DOI:** 10.1166/jnn.2012.5111
3. Kuchibhatla, S.V.N.T.; Karakoti, A.S.; Bera, D.; Seal, S.; *Prog. Mater. Sci.* **2007,** *52*, 699. **DOI:** 10.1016/j.pmatsci.2006.08.001
4. Patel, S.K.S.; Lee, J.H.; Kim, M.K.; Bhoi, B.; Kim, S.K.; *J. Mater. Chem. C* **2018,** *6*, 526. **DOI:** 10.1039/C7TC05362B
5. Hochbaum, A.I.; Yang, P.D.; *Chem. Rev.* **2010,***110*, 527. **DOI:** 10.1021/cr900075v
6. Yan, H.; Park, S.H.; Finkelstein, G.; Reif, J.H.; LaBean, T. H.; *Science* **2003,** *301*, 1882. **DOI:** 10.1126/science.1089389
7. Yan, R.X.; Gargas, D.; Yang, P. D.; *Nat. Photonics* **2009,** *3*, 569. **DOI:** 10.1038/nphoton.2009.184
8. Patel, S.K.S.; Dewangan, K.; Gajbhiye, N.S.; J. Mater. Sci. Tech. **2015,** *31*, 453. **DOI:** 10.1016/j.jmst.2014.08.013
9. Chhikara, D.; Srivatsa, K.M.K.; Kumar, M.S.; Singh, P.; Das, S.; Panwar, O.S.; Adv. Mater. Lett. 2015, 6(10), 862-866. **DOI:** 10.5185/amlett.2015.5886
10. Patra, R.; Sharma, H.; Singh, S.; Ghosh, S.; Vankar, V.D.; *Adv. Mat. Lett. 2014, 5(10), 573-577.* **DOI:** 10.5185/amlett.2014.5578
11. Chen, C.M.; Huang, J.Q., Zhang, Q.; Gong, W.Z.; Yang, Q.H.; Wang, M.Z.; et al. *Carbon* **2012**, *50*, 659. **DOI:** 10.1016/j.carbon.2011.09.022
12. Brezesinski, T.; Wang, J.; Tolbert, S.H.; Dunn, B.; *Nat. mater.* **2010,** *9*, 146. **DOI:** 10.1038/NMAT2612
13. Dewangan, K.; Sinha, N.N.; Sharma, P.K.; Pandey, A.C.; Munichandraiah, N.; Gajbhiye, N.S.; *CrystEngComm* **2011,** *13*, 927. **DOI:** 10.1039/C0CE00271B
14. Yan, B.; Zheng, Z.; Zhang, J.; Gong, H.; Shen, Z.; Huang W.; Yu, T.; *J. Phys.Chem. C* **2009,** *113*, 20259. **DOI:** 10.1021/jp907602w
15. Li, Y. B.; Bando, Y.; Golberg D.; Kurashima, K.; *Appl. Phys. Lett.*, **2002,** *81*, 5048. **DOI:** 10.1063/1.1532104
16. Wei, G.; Qin, W.; Zhang, D.; Wang, G.; Kim, R.; Zheng, K.; Wang, L.; J. Alloys Compd., **2009,** *481*, 417. **DOI:** 10.1016/j.jallcom.2009.03.007
17. Zhou, J.; Xu, N.-S; Deng, S.-Z.; Chen, J.; She, J.-C.; Wang, Z.-L.; *Adv. Mater.*, **2003,** *15*, 1835. **DOI:** 10.1002/adma.200305528
18. Wieghardt, K.; Dahmann, G.B.; Swiridoff, W.; Weiss, J.; *Inorg. Chem.*, **1983,** *22*, 1221. **DOI:** 10.1021/ic00150a016
19. Cullity, B.D.; 'Elements of X-ray Diffraction', 2nd Edition, Addison-Wesley, USA, **(1959)**.
20. Lupan O.; Trofim V.; Cretu V.; Stamov I.; Syrbu N.N.; Tiginyanu I.; Mishra Y.K.; Adelung R.; *J. Phys. D: Appl. Phys.* **2014,** *47*, 085302. **DOI:** 10.1088/0022-3727/47/8/085302
21. Navas I.; Vinodkumar R.; Lethy K.J.; Ganesan V.; Sathe V.; Mahadevan Pillai V.P.; *J. Phys. D: App. Phys.* **2009,** *42*, 175305. **DOI:** 10.1088/0022-3727/42/17/175305
22. Mestl G.*; J. Raman Spectroscopy* **2002,** *33*, 333–347. **DOI:** 10.1002/jrs.843
23. Chen, M.; Friend, C. M.; Kaxiras, E.; *J. Am. Chem. Soc.*, **2001,** *123*, 2224. **DOI:** 10.1021/ja994376s
24. Fowler, R.H.; Nordheim, L.; *R. Soc. London, Ser. A*, **1928,** *119*, 173. **DOI:** 10.1098/rspa.1928.0091
25. Zhou, J.; Deng, S.Z.; Xu, N.S.; Chen, J.; She, J.C.; *Appl. Phys. Lett.* **2003,** *83*, 653. **DOI:** 10.1063/1.1613992
26. Khademi, A.; Azimirad, R.; Zavarian, A.A.; Moshfegh, A.Z.; *J. Phys. Chem. C*, **2009,** *113*, 19298. **DOI:** 10.1021/jp9056237
27. Yook, K.S.; Lee, J.Y.; *Synth. Met.*, **2009,** *159*, 69. **DOI:** 10.1016/j.synthmet.2008.07.016
28. Matsushima, T.; Kinoshita, Y.; Murata, H.; *Appl. Phys. Lett.*, **2007,** *91*, 253504. **DOI:** 10.1063/1.2825275
29. Li, Z.-Y.; Wu, Q.-H.; *J. Mater. Sci.: Mater. Electronics*, **2008,** *19*, S366. **DOI:** 10.1007/s10854-007-9506-z
30. Schulz P.; Tiepelt J.O.; Christians J.A.; Levine I.; dri E. E.; Sanehira E.M.; Hodes G.; Cahen D.; Kahn A.; *ACS Appl. Mater. Interfaces* **2016,** *8*, 31491. **DOI:** 10.1021/acsami.6b10898

